



HAL
open science

Radiomic decision maps reveal patterns discriminating between glioma progression and radiation-induced necrosis in static and dual time [18F]-FDOPA PET

Thibault Escobar, Fanny Orlhac, Anne-Capucine Rollet, Olivier Humbert, Sebastien Vauclin, Pascal Pineau, Jacques Darcourt, Irene Buvat

► To cite this version:

Thibault Escobar, Fanny Orlhac, Anne-Capucine Rollet, Olivier Humbert, Sebastien Vauclin, et al.. Radiomic decision maps reveal patterns discriminating between glioma progression and radiation-induced necrosis in static and dual time [18F]-FDOPA PET. Society of Nuclear Medicine and Molecular Imaging meeting, Jun 2022, Vancouver, Canada. hal-04248818

HAL Id: hal-04248818

<https://hal.science/hal-04248818>

Submitted on 18 Oct 2023

HAL is a multi-disciplinary open access archive for the deposit and dissemination of scientific research documents, whether they are published or not. The documents may come from teaching and research institutions in France or abroad, or from public or private research centers.

L'archive ouverte pluridisciplinaire **HAL**, est destinée au dépôt et à la diffusion de documents scientifiques de niveau recherche, publiés ou non, émanant des établissements d'enseignement et de recherche français ou étrangers, des laboratoires publics ou privés.

Radiomic decision maps reveal patterns discriminating between glioma progression and radiation-induced necrosis in static and dual time [18F]-FDOPA PET

Thibault Escobar, Fanny Orlhac, Anne-Capucine Rollet, Olivier Humbert, Sebastien Vauclin, Pascal Pineau, Jacques Darcourt and Irene Buvat

Introduction: Differential diagnosis between glioma progression and treatment-related radionecrosis using MRI is often difficult [1]. Recent studies have shown the potential of dynamic and dual time [18F]-FDOPA PET as well as radiomics in this context [2, 3]. Yet, the image information on which radiomic models are based remain unclear. In this work, we used a method combining voxel-wise radiomic features and importance maps [4] to understand the models and highlight the patterns specifically associated with tumor radionecrosis.

Methods: Ninety-six studies from 87 patients with suspicious uptake in [18F]-FDOPA PET were used. Each study included 2 static PET/CT scans: performed at 20 min (PET-20) and at 90 min (PET-90) post-injection. Final diagnosis of progression or radionecrosis was based on a 6-month follow-up and pathological data when available. PET-20 and PET-90 images were rigidly registered. The tumor and the contralateral striatum were segmented using a threshold set to 50% of the striatum SUVmax on PET-20 and propagated to PET-90. PET-20 and PET-90 images were scaled to the patient striatum uptake SUVmax or SUVmean by computing tumor to striatum uptake ratio to yield striatum-standardized images (SSI) [5, 6], denoted SSImax-20, SSImean-20, SSImax-90, and SSImean-90. Dual time point images were obtained by subtracting the 90 min images from the 20 min images, leading to PET-20-90, SSImax-20-90, and SSImean-20-90. A total of 924 voxel-wise radiomic feature maps were extracted by sliding a $5 \times 5 \times 5$ -voxel kernel over each image. The mean value over the tumor ROI was used for each feature to yield two feature vectors per patient, one for all images (924 features) and the other only for the standard 20 min images (231 features) to assess the added value of the dual time approach. After reducing redundancy using the variance inflation factor, we built two probabilistic models, M-20 and M-dual-time, to identify radionecrosis using forward feature selection and bagging regularized logistic regression. Radiomic decision maps (RDM) were computed by backprojecting the decision functions of the models at the voxel level. Based on the RDMs interpretation, we defined a simple and interpretable voxel-level 2D feature space for each model. We finally plotted 10,000 voxels randomly sampled from the whole dataset in these 2D spaces, colored by their predicted decision values and patient number to highlight the interpretations.

Results: There were 69 progressions and 27 radionecroses. Through cross-validation, 3 and 5 features were selected for M-20 and M-dual-time with a mean balanced accuracy of $71 \pm 9\%$ (permutation test p-value = 0.04) and $75 \pm 9\%$ (p-value = 0.03) respectively, with no significant difference between the 2 models. Sensitivity, specificity, and AUROC are reported

in Table 1. Dual time features were preferentially selected by the model when available (4/5 features of M-dual-time). SSI features were also preferentially selected by both models (3/3 for M-20, 3/5 for M-dual-time). By interpreting the RDMs together with the models equations and then creating the 2D voxel-level feature spaces, we found that low local tumor to striatum uptake ratio was predictive of radionecrosis when using only the 20 min images, while radionecrosis identification was based on a locally homogeneous slow tracer wash-out when the 2 time points were used, consistently with other recent image-based studies [2, 7, 8].

Conclusions: Using RDMs for interpreting radiomic models built from a limited number of patients, our data-driven approach highlighted two patterns that discriminate radionecrosis from tumor progression without significant difference in terms of classification performances: low tumor to striatum uptake ratio at 20 min and locally homogeneous slow wash-out between 20 min and 90 min.

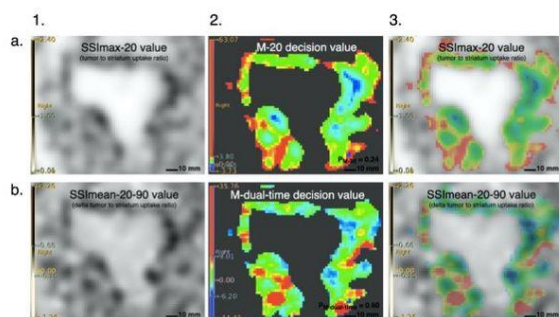


Figure 1. Example of Radiomic Decision Maps (RDM) for patient 79 (radionecrosis). First row (a): model M-20 based on PET images performed at 20 min only. (1) SSImax-20 image, (2) M-20 RDM, (3) M-20 RDM overlaid on SSImax-20 image. Second row (b): model M-dual-time based on static and dual time PET images. (1) SSImean-20-90 image, (2) M-dual-time RDM, (3) M-dual-time RDM overlaid on SSImean-20-90 image. The RDM signal is high (red) when the voxel increases the predicted probability of radionecrosis and is low (blue) when the voxel increases the probability of progression.

$$\begin{aligned}
 & -0.326 (0.375) \times \text{Local Minimum SSImax-20} \\
 & -0.624 (0.346) \times \text{SDLGLE SSImax-20} \\
 & 0.844 (0.385) \times \text{GLCM Joint Energy SSImean-20} \\
 & -0.150 (0.104)
 \end{aligned}$$

Equation 1. Decision function of the bagging logistic model M-20 with standard deviation of the coefficients.

$$\begin{aligned}
 & -0.516 (0.301) \times \text{LDLGLE PET-90} \\
 & -1.016 (0.380) \times \text{Local Median PET-20-90} \\
 & 0.309 (0.342) \times \text{Local Skewness SSImean-20-90} \\
 & 1.319 (0.472) \times \text{LDE SSImean-20-90} \\
 & -0.564 (0.334) \times \text{GLCM ldn SSImax-20} - \text{GLCM ldn SSImax-90} \\
 & -0.396 (0.218)
 \end{aligned}$$

Equation 2. Decision function of the bagging logistic model M-dual-time with standard deviation of the coefficients.

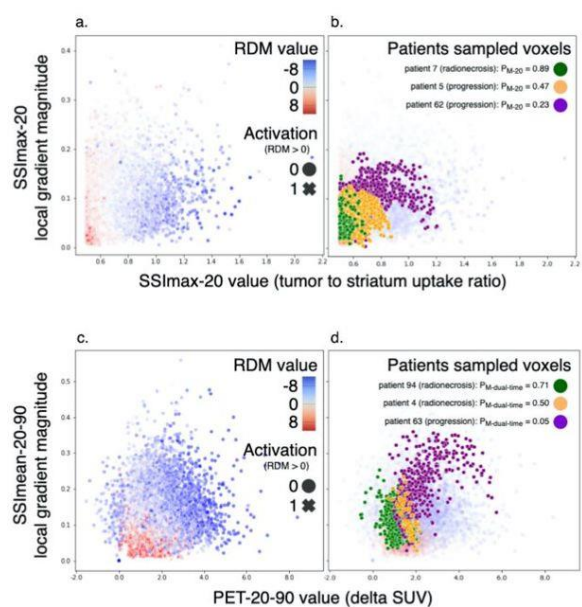


Figure 2. Plot of 10000 voxels randomly sampled from the whole dataset in the voxel-level 2D feature spaces, colored by their predicted decision values with 6 patients highlighted (green, purple, orange in each graph). (a, b) M-20. (c, d) M-dual-time. The local gradient magnitude was used (y-axis) as it reflects the local heterogeneity in an image in a simple and interpretable way. At 20 min, high radionecrosis probability (red points in a) is essentially associated with low tumor to striatum uptake ratio (green patient in b). In the dual time context, high radionecrosis probability (red points in c) is associated with low tumor to striatum uptake ratio (green patient in d) and homogeneous (low local gradient magnitude) wash-out (green patient in d).